

ORIGINAL RESEARCH

Echocardiographic Features of Wild-Type Transthyretin Cardiac Amyloidosis From J-Case

Multicenter Survey in Japan



Shuichi Kitada, MD, PhD,^a Yu Kawada, MD, PhD,^a Yasuhiro Shintani, MD, PhD,^a Junki Yamamoto, MD, PhD,^a Shohei Kikuchi, MD, PhD,^a Hiroki Usuku, MD, PhD,^b Kenichi Tsujita, MD, PhD,^b Yuri Ochi, MD, PhD,^c Toru Kubo, MD, PhD,^c Hirohiko Motoki, MD, PhD,^d Hiroyuki Iwano, MD, PhD,^e Takatomo Watanabe, MD, PhD,^f Nobuyuki Ohte, MD, PhD,^g Yoshihiro Seo, MD, PhD^a

ABSTRACT

BACKGROUND Wild-type transthyretin cardiac amyloidosis (ATTRwt-CA) occurs at a high prevalence in older patients with left ventricular (LV) hypertrophy. However, detecting ATTRwt-CA using echocardiography is challenging.

OBJECTIVES This study identified echocardiographic findings characterizing ATTRwt-CA compared with monoclonal immunoglobulin light chain cardiac amyloidosis (CA) and hereditary transthyretin CA.

METHODS We conducted a multicenter, retrospective study on the echocardiographic findings characterizing ATTRwt-CA. J-CASE (Japan Cardiac Amyloidosis Survey of typical Echocardiographic findings) analyzed echocardiographic data in 311 patients with histologically proven amyloid deposition in the myocardium and diagnosis of transthyretin CA or monoclonal immunoglobulin light chain CA.

RESULTS Among the cohort, 172 patients (55.3%) were diagnosed with ATTRwt-CA. A multiple discriminant analysis revealed that LV hypertrophy with a more extensive LV mass index but relatively modest interventricular septum thickening and enlargement of maximal papillary muscle diameter were significant echocardiographic findings characterizing ATTRwt-CA. In addition to the patient backgrounds such as advanced age, male sex, concomitant diabetes mellitus, hyperlipidemia, carpal tunnel syndrome, and paroxysmal atrial fibrillation, the discriminant model, including these echocardiographic findings showed significant discriminant power of ATTRwt-CA from the other subtypes (83.8% accuracy with 86.0% positive predictive value and 81.4% negative predictive value, when the sensitivity and specificity are at their maximum values of the model).

CONCLUSIONS In the J-CASE data set, LV hypertrophy with a more extensive LV mass index but relatively modest interventricular septum thickening and enlargement of papillary muscle diameter significantly characterized ATTRwt-CA. These findings may lead to more accurate screening echocardiography for diagnosing ATTRwt-CA and motivate the subsequent comprehensive clinical diagnostic process, including multimodality imaging. (JACC Asia. 2025;5:633-646)
© 2025 The Authors. Published by Elsevier on behalf of the American College of Cardiology Foundation. This is an open access article under the CC BY-NC-ND license (<http://creativecommons.org/licenses/by-nc-nd/4.0/>).

From the ^aDepartment of Cardiology, Nagoya City University Graduate School of Medical Sciences, Nagoya, Japan; ^bDepartment of Cardiovascular Medicine, Graduate School of Medical Sciences, Kumamoto University, Kumamoto, Japan; ^cDepartment of Cardiology and Geriatrics, Kochi Medical School, Kochi University, Kochi, Japan; ^dDepartment of Cardiovascular Medicine, Shinshu University School of Medicine, Matsumoto, Japan; ^eDivision of Cardiology, Teine Keijinkai Hospital, Sapporo, Japan; ^fDepartment of Cardiology, Gifu University Graduate School of Medicine, Gifu, Japan; and the ^gDepartment of Cardiology, Nagoya City University East Medical Center, Nagoya, Japan.

**ABBREVIATIONS
AND ACRONYMS****AL-CA** = monoclonal immunoglobulin light chain cardiac amyloidosis**ATTRv-CA** = hereditary/variant transthyretin cardiac amyloidosis**ATTRwt-CA** = wild-type transthyretin cardiac amyloidosis**BNP** = brain natriuretic peptide**IVST** = interventricular septum thickness**LA** = left atrial**LVEF** = left ventricular ejection fraction**LVMI** = left ventricular mass index**PWT** = posterior wall thickness**RV** = right ventricular

Cardiac amyloidosis (CA) is an infiltrative cardiomyopathy caused by amyloid deposition in the myocardium. Two protein precursors are known to be the primary causes of CA: monoclonal immunoglobulin light chain amyloidosis (AL), which is produced by bone marrow plasma cells, and transthyretin (TTR), which is synthesized primarily by the liver.^{1,2} The amyloidosis caused by amyloid transthyretin (ATTR) is further subtyped into wild-type transthyretin (ATTRwt) or hereditary/variant transthyretin (ATTRv) based on genetic variants in the TTR gene.³ Significant management issues in CA are that the prognosis remains poor for both AL- and ATTR-CA. Untreated AL-CA has an average survival of <6 months, and ATTRwt-CA has a reported survival of 2 to 3 years after diagnosis.^{4,5} Recently, the ATTR-ACT (Transthyretin Amyloidosis Cardiomyopathy Clinical Trial)

showed that administration of tafamidis for ATTR-CA was associated with reductions in all-cause mortality and cardiovascular-related hospitalizations compared with placebo,⁶ making it an important treatment option for patients with ATTRwt-CA.

According to previous reports, ATTRwt-CA is more common than generally thought, with a prevalence as high as 10% in older patients with left ventricular (LV) hypertrophy, 14% in patients with heart failure with preserved ejection fraction, and up to 15% in older patients with aortic stenosis.^{7,8} ATTRwt-CA is a crucial background disease for differential diagnosis of heart failure in older patients, because it is a late-onset disease. However, detecting ATTRwt-CA remains a significant challenge, and several researchers have discussed the early clinical signs and associated features of ATTRwt-CA, proposing a diagnostic algorithm.⁹⁻¹¹ Besides, the usefulness of technetium-99m-pyrophosphate or hydroxymethylene diphosphonate myocardial scintigraphy in diagnosing ATTRwt-CA has been demonstrated with high diagnostic sensitivity and specificity. If AL-CA can be ruled out in the patients suspected of CA, the diagnostic sensitivity and specificity will be even higher.⁹ Therefore, the key to diagnosing ATTRwt-CA is first to suspect CA, then rule out AL-CA using screening

a monoclonal component in serum or urine, and finally perform technetium-99m-pyrophosphate or hydroxymethylene diphosphonate myocardial scintigraphy on the patients suspected of CA. In any diagnostic proposal, echocardiography, which is at the forefront of solving this problem, holds great promise. However, echocardiographic assessment still does not play a sufficient role in its diagnostic process.¹² A thorough knowledge of the echocardiographic findings characteristic of ATTRwt-CA would lead to more accurate screening echocardiography for diagnosing ATTRwt-CA and motivate the subsequent diagnostic process.

Therefore, we conducted a multicenter, retrospective study on the echocardiographic findings characterizing ATTRwt-CA by analyzing the echocardiographic data in patients with histologically proven amyloid deposition in the myocardium. This study aimed to identify echocardiographic findings that differentiate ATTRwt-CA from AL- and ATTRv-CA.

METHODS

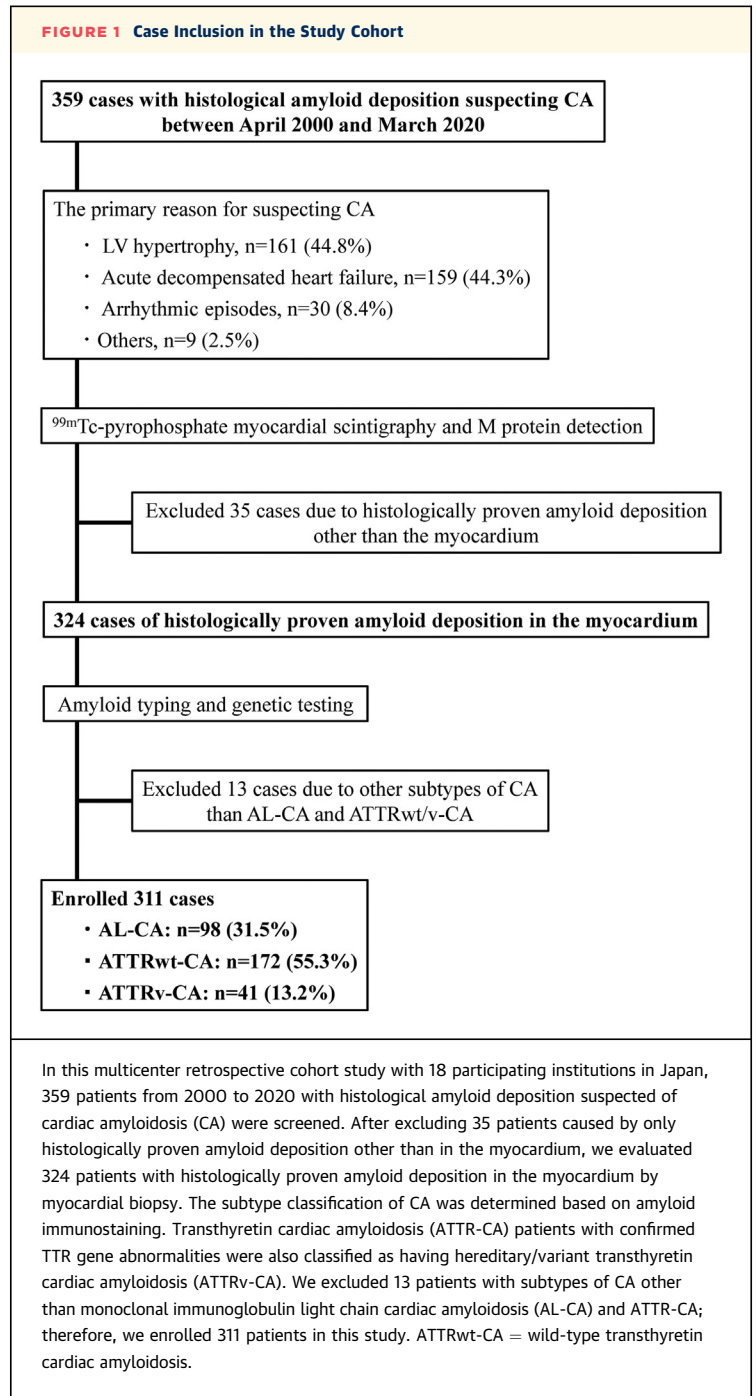
STUDY COHORT AND DATA COLLECTION. J-CASE (Japan Cardiac Amyloidosis Survey of typical Echocardiographic findings) is a multicenter retrospective cohort study with 18 participating institutions in Japan. From 2000 to 2020, 359 patients with histological amyloid deposition suspected of CA were screened. After excluding 35 patients because of only histologically proven amyloid deposition other than in the myocardium, we evaluated 324 patients with histologically proven amyloid deposition in the myocardium by myocardial biopsy. The subtype classification of CA was determined based on amyloid immunostaining. ATTR-CA patients with confirmed TTR gene abnormalities were also classified as having ATTRv-CA. We excluded 13 patients with subtypes of CA other than AL- and ATTR-CA (4 cases, amyloid A amyloidosis; 1 case, β 2-microglobulin-related amyloidosis; 1 case, isolated atrial amyloidosis; 3 cases with 2 or more mixed subtypes; 4 cases with a difficult immunological diagnosis). Therefore, we enrolled 311 patients in this study (Figure 1). We gathered information on the patients' characteristics, including age, gender, body mass index, heart failure symptoms indicated by the NYHA functional

The authors attest they are in compliance with human studies committees and animal welfare regulations of the authors' institutions and Food and Drug Administration guidelines, including patient consent where appropriate. For more information, visit the [Author Center](#).

Manuscript received April 17, 2024; revised manuscript received January 2, 2025, accepted January 6, 2025.

classification, basic cardiac rhythm, comorbidities, and brain natriuretic peptide (BNP) levels at the time of histological diagnosis of CA as the baseline for this study. In addition, 2-dimensional echocardiographic images taken at an acceptable range of 1 month before and after baseline were collected in DICOM format and analyzed in the core laboratory using TOMTEC-ARENA 4.6 (TomTec Imaging Systems). This retrospective study was conducted in accordance with the Declaration of Helsinki, and it received approval from the Institutional Review Boards and Ethics Committees at all sites. We adopted an opt-out approach to notify eligible patients of the research use of their information before enrollment.

ACQUISITION OF ECHOCARDIOGRAPHY. Following the recommendations on echocardiographic assessment from the American Society of Echocardiography and the European Association of Cardiovascular Imaging (ASE/EACVI),¹³⁻¹⁸ skilled sonographers blinded to the patient's information evaluated the available M-mode, B-mode, color, pulsed-, and continuous-wave Doppler; tissue Doppler; and speckle tracking imaging data for each patient. They measured cardiac chamber size; left ventricular ejection fraction (LVEF) using the Simpson biplanar method; LV diastolic functions following the grading algorithm of the 2016 ASE/EACVI recommendations using the mitral flow velocities of E and A waves, mitral annular e' velocity, E/e' ratio, peak velocity of tricuspid regurgitation velocity, and left atrial (LA) maximum volume index; right ventricular (RV) functions, including RV fractional area change, tricuspid annular plane systolic excursion, and RV free-wall strain; and LA reservoir, conduit, and booster strains using apical 4-chamber view and R to R gating of the cardiac cycle on electrocardiography. Stroke volume was calculated using the LV outflow tract diameter and flow velocity time integral. Sigmoid septum was defined as basal interventricular septum (IVS) hypertrophy (interventricular septum thickness [IVST] ≥ 13 mm for men, ≥ 12 mm for women) and $<120^\circ$ angle from the anterior wall of the aorta to the IVS surface in a parasternal long-axis image. The presence of a granular sparkling appearance, which is attributed to increased echogenicity because of the deposition of amyloid,¹⁹ was determined by 2 skilled sonographers on the same image. Significant pericardial effusion was present if the pericardial cavity was enlarged >10 mm at end-diastole at the papillary muscle level of the parasternal short-axis image. Regarding the severity of valvular disease, significant valvular disease was defined as more than moderate based on the



Japanese guidelines for the treatment of valvular disease.²⁰ A mitral annulus calcification was considered significant if it was present in more than one-half of the mitral annulus. The maximum mitral valve thickness at the mitral valve opening in the parasternal long-axis image was used for mitral valve thickness. For the size of the mitral papillary muscle, the largest diameter of the anterior or posterior

TABLE 1 Comparison of Clinical Backgrounds Among the 3 Groups

	ATTRwt-CA (n = 172)	AL-CA (n = 98)	ATTRv-CA (n = 41)	P Value
Age, y	77 ± 6 ^{a,b}	66 ± 10	62 ± 14	<0.001
Male, %	146/172 (84.9) ^{a,b}	60/98 (61.2)	23/41 (56.1)	<0.001
BSA, m ²	1.62 ± 0.15	1.61 ± 0.17	1.59 ± 0.17	0.681
NYHA functional class ≥II	135/158 (85.4)	76/89 (85.4)	12/17 (70.6)	0.263
Non-sinus rhythm, %	55/169 (32.5) ^{a,b}	8/98 (8.2)	9/41 (22.0)	<0.001
Comorbidity, %				
Hypertension	95/172 (55.2) ^{a,b}	34/98 (34.7)	7/41 (17.1)	<0.001
Diabetes mellitus	43/172 (25.0) ^{a,b}	14/98 (14.3)	3/41 (7.3)	0.011
Hyperlipidemia	52/172 (30.2) ^{a,b}	17/98 (17.3)	3/41 (7.3)	0.002
History of CAD	13/172 (7.6)	4/98 (4.1)	0/41 (0.0)	0.123
History of stroke	3/172 (1.1)	7/98 (7.9)	4/41 (33.3)	0.172
On hemodialysis	4/172 (2.3)	4/98 (4.1)	1/41 (2.4)	0.698
Carpal tunnel syndrome	59/172 (34.3) ^{a,b}	7/98 (7.1)	7/40 (17.5)	<0.001
Paroxysmal AF	57/172 (33.1) ^{a,b}	15/98 (15.3)	3/41 (7.3)	<0.001
Ventricular arrhythmia	21/171 (12.3)	11/98 (11.2)	0/41 (0.0)	0.063
Bradyarrhythmia	23/172 (13.4)	13/98 (13.3)	7/41 (17.1)	0.811
Laboratory data				
Log BNP, pg/mL	5.65 ± 0.75 ^{a,b}	6.05 ± 1.22 ^b	4.48 ± 1.13	<0.001

Values are mean ± SD or n/N (%). ^avs monoclonal immunoglobulin light chain cardiac amyloidosis (AL-CA); *P* < 0.05. ^bvs hereditary/variant transthyretin cardiac amyloidosis (ATTRv-CA); *P* < 0.05.
AF = atrial fibrillation; ATTRwt/v = wild-type transthyretin cardiac amyloidosis; BNP = brain natriuretic peptide; BSA = body surface area; CA = cardiac amyloidosis; CAD = coronary artery disease.

papillary muscles was adopted in the image where the papillary muscle could best be observed in the parasternal short-axis image. Finally, the relative apical sparing pattern of the basal and mid-segmental longitudinal strain (LS) to the apical LS in the LV was evaluated by the apical-sparing index, which was defined as follows: average apical LS/(average basal LS + average mid-LS).²¹

STATISTICAL ANALYSIS. Continuous data are presented as the mean ± SD, although BNP levels were expressed in natural logarithms, and categorical variables were summarized as frequencies and percentages. Continuous variables were compared among the 3 groups using 1-way analysis of variance (ANOVA) when normality was found in each group by the Shapiro-Wilk test. When normality was not found, the Kruskal-Wallis test was used for the comparison. Post hoc testing was conducted when a significant difference was found in the 3 groups' comparisons by 1-way ANOVA or Kruskal-Wallis methods. The post hoc testing that followed the 1-way ANOVA was conducted using the Tukey method when homogeneity of variance was assumed and the Tamhane method when homogeneity was not. Besides, the post hoc testing that followed the Kruskal-Wallis methods was carried out by the Dunn-Bonferroni method with correction for multiple tests. The categorical variables

were compared by Pearson's chi-square test or Fisher exact test. *P* < 0.05 was considered significant. We used a multiple discriminant analysis to determine the clinical backgrounds and echocardiographic findings that differentiate ATTRwt-CA from AL- and ATTRv-CA. In univariate discriminant analysis, we selected clinical backgrounds and echocardiographic findings with high discriminant probability (*Z* value ≥55%). Then, we examined discriminant factors differentiating ATTRwt-CA from the other subtypes in a multiple discriminant analysis using a step-wise procedure. In addition, we provided a figure showing a diagnostic performance plot (DP-plot) of the model with discriminant factors with *F*-value ≥2.0 in the multiple discriminant analysis. And then, we provided the receiver-operating characteristic curve of the model at the optimal discriminant score where the theoretical sensitivity and specificity match. All statistical analyses were performed in SPSS version 29.0 software (SPSS Japan Inc) and R statistical software (R Foundation for Statistical Computing).

RESULTS

PATIENT CHARACTERISTICS. Of 359 patients suspected of CA, 44.8% (n = 161) were mainly suspected because of LV hypertrophy, 44.3% (n = 159) because of congestive heart failure, and 8.4% (n = 30) because of arrhythmic episodes. A total of 311 patients histologically proven to have AL-CA (n = 98, 31.5%), ATTRwt-CA (n = 172, 55.3%), or ATTRv-CA (n = 41, 13.2%) were enrolled in this study (Figure 1). The mean patient age was 72 years, and 73.6% were men. More than 70% (71.7%) of the patients had heart failure symptoms (the NYHA functional class ≥II), median BNP levels were 295.1 pg/mL, and the mean LVEF was 49.0%. A comparison of patient characteristics among the 3 groups is provided in Table 1. Compared with the AL- and ATTRv-CA groups, the ATTRwt-CA group was significantly older and more likely to be men. They also more frequently presented with non-sinus rhythm and hypertension, diabetes mellitus, hyperlipidemia, carpal tunnel syndrome, or paroxysmal atrial fibrillation as comorbidities. Furthermore, the ATTRwt-CA group had significantly higher BNP levels than the ATTRv-CA group but lower levels than the AL-CA group.

ECHOCARDIOGRAPHIC FINDINGS CHARACTERIZING ATTRwt-CA. Echocardiographic findings associated with LV morphological changes, LV function parameters, morphological and functional changes in the RV and both atria, and degeneration of heart valves in CA were investigated and compared between

TABLE 2 Comparison of Echocardiographic Parameters Among the 3 Groups

	ATTRwt-CA (n = 172)	AL-CA (n = 98)	ATTRv-CA (n = 41)	P Value
LV volume and hypertrophy				
LVDD, mm	41.5 ± 6.5	40.0 ± 6.0	40.4 ± 4.4	0.111
LVDS, mm	31.9 ± 6.9 ^{a,b}	28.4 ± 6.6	28.5 ± 4.9	<0.001
IVST, mm	15.1 ± 3.1 ^a	13.7 ± 3.0	14.9 ± 3.4	0.003
IVST/PWT ratio	0.96 ± 0.16 ^b	0.98 ± 0.17 ^b	1.09 ± 0.17	<0.001
PWT, mm	16.0 ± 3.5 ^{a,b}	14.2 ± 3.0	13.8 ± 3.1	<0.001
LVEDVI, mL/m ²	53.8 ± 18.0	54.2 ± 17.7	54.4 ± 19.3	0.971
LVESVI, mL/m ²	29.0 ± 13.8	27.8 ± 12.9	25.4 ± 11.8	0.302
LVMI, g/m ²	163.7 ± 51.6 ^{a,b}	129.8 ± 32.5	142.1 ± 42.7	<0.001
RWT	0.80 ± 0.25 ^b	0.74 ± 0.22	0.70 ± 0.19	0.016
Normal LV wall thickness ^c	11/170 (6.5) ^a	17/95 (17.9)	6/41 (14.6)	0.013
Sigmoid septum	37/171 (21.6)	19/97 (19.6)	4/41 (9.8)	0.225
Granular sparkling	140/170 (82.4)	71/97 (73.2)	34/41 (82.9)	0.172
Pericardial effusion	12/171 (7.0)	7/96 (7.3)	3/41 (7.3)	0.995
LV function				
LVEF, %	47.4 ± 11.5 ^b	49.8 ± 11.2	53.8 ± 10.9	0.004
SV index, mL/m ²	32.1 ± 11.0 ^b	32.5 ± 13.8 ^b	35.7 ± 8.1	0.026
E-wave, cm/s	79.2 ± 22.2	86.0 ± 25.8 ^b	74.6 ± 23.2	0.017
A-wave, cm/s ^d	56.6 ± 28.8 ^b	59.4 ± 26.1 ^b	75.5 ± 23.7	0.001
Duration of A-wave, ms	156.3 ± 37.7	151.4 ± 33.4	155.1 ± 34.4	0.413
Deceleration time of E-wave, ms	188.6 ± 58.7 ^b	191.8 ± 66.0	228.7 ± 86.6	0.002
E/A ^d	1.82 ± 1.29 ^b	1.77 ± 1.09 ^b	1.15 ± 0.75	0.001
e' sep, cm/s	3.7 ± 1.2 ^{a,b}	4.3 ± 1.5	4.7 ± 1.8	<0.001
e' late, cm/s	5.2 ± 1.9 ^b	5.2 ± 1.9 ^b	6.7 ± 3.1	0.024
a' sep, cm/s	4.4 ± 2.0 ^b	5.2 ± 2.6 ^b	6.7 ± 2.6	<0.001
a' late, cm/s	4.8 ± 2.1 ^{a,b}	6.0 ± 3.0	6.6 ± 2.7	0.013
s' sep, cm/s	4.5 ± 1.7 ^{a,b}	5.8 ± 1.9	5.4 ± 1.7	<0.001
s' late, cm/s	5.3 ± 1.7 ^a	6.4 ± 2.7	6.4 ± 2.4	0.001
E/e' average	19.6 ± 8.8	20.2 ± 10.6	15.4 ± 6.5	0.172
LV diastolic dysfunction ^e	79/128 (61.7)	57/87 (65.5)	16/37 (43.2)	0.061
LV longitudinal strain				
Global, %	-10.1 ± 3.6 ^b	-10.6 ± 4.4 ^b	-14.2 ± 4.0	<0.001
Base, %	-6.2 ± 3.6 ^b	-7.2 ± 4.5 ^b	-10.9 ± 4.4	<0.001
Mid, %	-8.7 ± 3.9 ^b	-9.7 ± 4.8 ^b	-13.4 ± 4.7	<0.001
Apex, %	-14.7 ± 6.0 ^b	-14.3 ± 6.1 ^b	-18.4 ± 6.3	0.001
Apical sparing index	1.14 ± 0.63 ^b	0.99 ± 0.63	0.81 ± 0.29	0.003
LV circumferential strain				
Global, %	-18.6 ± 7.0 ^b	-20.7 ± 7.2	-21.9 ± 5.5	0.010
Base, %	-12.8 ± 7.3 ^{a,b}	-17.2 ± 8.4	-18.1 ± 5.3	<0.001
Mid, %	-18.6 ± 7.3 ^{a,b}	-20.9 ± 7.1	-23.5 ± 6.1	<0.001
Apex, %	-22.9 ± 9.7	-24.1 ± 9.4	-23.5 ± 8.0	0.660
RV volume and function				
RVDD base, mm	36.3 ± 6.9 ^a	33.9 ± 6.7	34.9 ± 7.1	0.028
RVDD mid, mm	26.5 ± 5.3	24.9 ± 5.9	24.9 ± 5.1	0.046
RVDD longitudinal, mm	68.3 ± 10.8	65.9 ± 9.9 ^b	71.4 ± 11.9	0.023
RVWT, mm	5.3 ± 1.6 ^b	5.3 ± 1.5 ^b	4.0 ± 1.4	<0.001
RVEDA, cm ²	17.2 ± 4.5	16.9 ± 6.3	16.5 ± 3.8	0.746
RVESA, cm ²	11.8 ± 3.8	11.6 ± 5.1	10.8 ± 3.6	0.381
RVFAC, %	31.4 ± 10.6	32.4 ± 9.6	35.3 ± 12.4	0.130
TAPSE, mm	14.3 ± 5.1	15.6 ± 4.9	15.5 ± 4.4	0.459
RVFWS, %	-13.0 ± 5.5 ^b	-14.0 ± 6.0 ^b	-17.3 ± 6.8	0.001

Continued on the next page

TABLE 2 Continued				
	ATTRwt-CA (n = 172)	AL-CA (n = 98)	ATTRv-CA (n = 41)	P Value
Atrial volume and function				
LAD, mm	41.3 ± 6.9 ^{a,b}	39.1 ± 7.2	36.5 ± 6.4	<0.001
LAVI, mL/m ²	47.9 ± 16.8 ^a	42.3 ± 17.2	41.0 ± 13.7	0.010
RAESA, cm ²	19.4 ± 6.3 ^{a,b}	17.5 ± 6.7	16.4 ± 4.8	0.003
IAST, mm	8.4 ± 2.6	8.0 ± 2.7	7.1 ± 2.2	0.131
LA strain				
Reservoir, %	13.0 ± 7.0 ^b	15.3 ± 8.0 ^b	21.2 ± 9.4	<0.001
Conduit, %	8.7 ± 4.1 ^b	9.3 ± 5.0 ^b	12.7 ± 6.1	<0.001
Booster, %	6.0 ± 5.1 ^b	6.4 ± 4.7 ^b	9.7 ± 5.9	<0.001
Valvular disease				
≥moderate AS	14/171 (8.2) ^a	0/95 (0.0)	0/41 (0.0)	0.003
≥moderate AR	10/172 (5.8)	1/95 (1.1)	0/41 (0.0)	0.056
≥moderate MS	1/172 (0.6)	0/96 (0.0)	0/41 (0.0)	0.671
≥moderate MR	35/172 (20.3) ^b	11/96 (11.5)	1/41 (2.4)	0.008
MAC	1/172 (0.6)	1/96 (1.0)	1/41 (2.4)	0.550
MV thickness, mm	3.3 ± 1.1 ^b	3.2 ± 1.2 ^b	2.7 ± 0.7	0.006
Papillary muscle, mm	13.5 ± 3.2 ^a	11.8 ± 2.6	12.6 ± 2.5	0.001
<p>Values are mean ± SD or n/N (%). ^avs AL-CA; P < 0.05. ^bvs ATTRv-CA; P < 0.05. ^cboth IVST and PWT were ≤12 mm. ^dData of 239 patients, excluding 2 patients because of unavailability of transmitral flow images, and 70 patients because of rhythms other than sinus. ^eLV diastolic dysfunction grade II or III.</p> <p>AR = aortic regurgitation; AS = aortic stenosis; E/A = the ratio between E-wave and A-wave of transmitral flow velocity; E/e' = ratio between early mitral inflow velocity and mitral annular early diastolic velocity; IAST = interatrial septum thickness; IVST = interventricular septal thickness; LAD = left atrial dimension; LAVI = left atrial volume index; LVDD = left ventricular end-diastolic diameter; LVDS = left ventricular end-systolic diameter; LVEDVI = left ventricular end-diastolic volume index; LVEF = left ventricular ejection fraction; LVESVI = left ventricular end-systolic volume index; LVMI = left ventricular mass index; MAC = mitral annular calcification; MR = mitral regurgitation; MS = mitral stenosis; MV = mitral valve; PWT = posterior wall thickness; RAESA = right atrial end-systolic area; RVDD = right ventricular end-diastolic diameter; RVEDA = right ventricular end-diastolic area; RVESA = right ventricular end-systolic area; RVFAC = right ventricular fractional area change; RVFWS = right ventricular free-wall strain; RVWT = right ventricular wall thickness at the base of the tricuspid valve in the long-axis image; RWT = relative wall thickness; TAPSE = tricuspid annular plane systolic excursion.</p>				

ATTRwt-CA and the other subtype of CA. Detailed values and comparative results for the echocardiographic findings are provided in [Table 2](#).

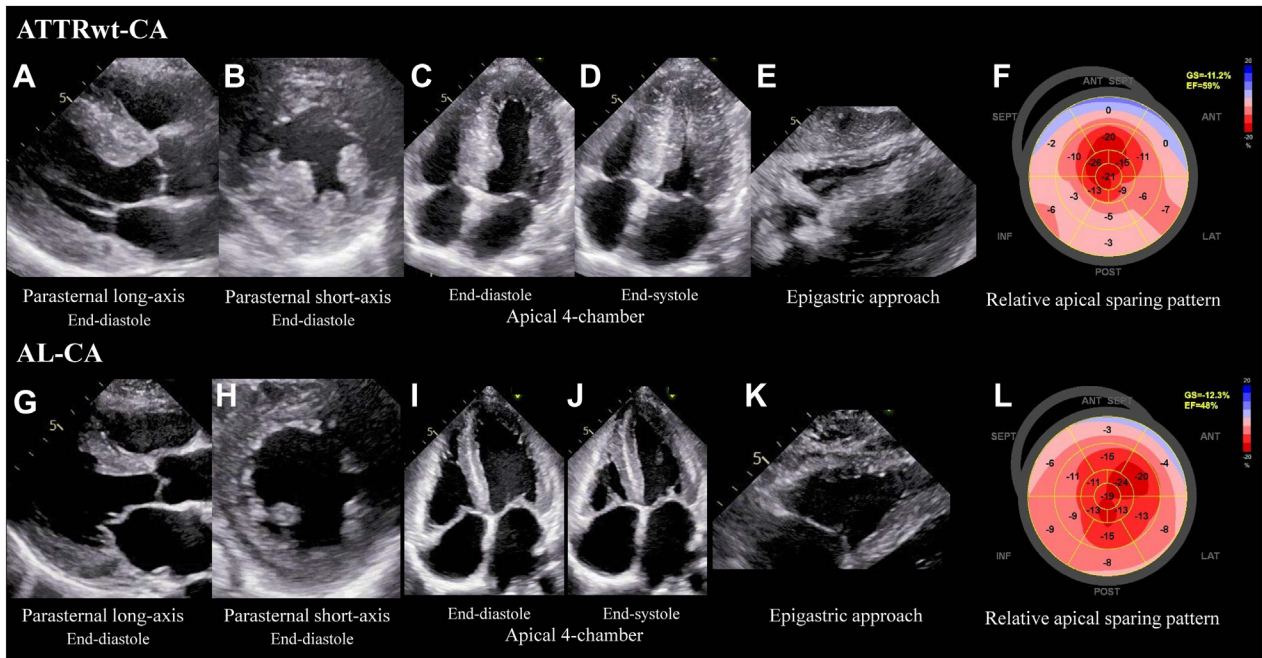
Important points to note: compared with the AL-CA group ([Figure 2](#)), the ATTRwt-CA group showed significant LV hypertrophy with significantly larger IVST, posterior wall thickness (PWT), and LV mass index; mitral papillary muscle hypertrophy with significantly larger maximal muscle diameter; enlargement of RV with larger basal RV end-diastolic diameter; and both atrial sizes with significantly larger LA volume index and RA end-systolic area. Notably, compared with those with AL-CA, a significantly smaller proportion presented normal LV wall thickness (IVST and PWT ≤12 mm). The LV systolic and diastolic function parameters and LA strain parameters were not different from those of the AL-CA group. In contrast, their apical-sparing index tended to be higher than the AL-CA group.

Besides, compared with the ATTRv-CA group, the ATTRwt-CA group also showed significant ventricular hypertrophy with significantly larger PWT, LV mass index, relative wall thickness, and RV wall thickness, and enlargement of both atrial sizes with significantly larger LA diameter and RA end-systolic area. Notably,

more significant LV asymmetry was observed in the ATTRv-CA group than in theirs. Regarding LV systolic and diastolic function parameters, they had significantly lower LVEF levels and stroke volume index. They also had a significantly lower A wave, resulting in a higher E/A ratio. Besides, the deceleration time of the E wave was significantly shorter in the ATTRwt-CA group. In contrast, the E/e' ratio difference did not reach significance between the 2 groups. The proportion of patients with LV diastolic dysfunction grade 2 or 3 showed a tendency to be higher than the ATTRv-CA group but did not reach statistical significance.

Regarding whole strain parameters, LV LS and circumferential strains, LA strains, and RV free-wall strains were significantly reduced in the ATTRwt-CA group. However, in this study, the mean age of the ATTRwt-CA group was significantly higher than the other 2 groups (age 77 ± 6 years vs 66 ± 10 years in AL-CA and 62 ± 14 years in ATTRv-CA) ([Table 1](#)), which may be related to the reduced strain values in the ATTRwt-CA group. Regarding the apical-sparing index, they showed a significantly higher index than the ATTRv-CA group. Besides, they showed a significantly increased mitral valve thickness and a higher concurrence rate of more than moderate mitral

FIGURE 2 Comparison of Echocardiographic Findings Between ATTRwt-CA and AL-CA



Typical echocardiographic findings of ATTR-CA and AL-CA are shown. Compared with the AL-CA group, the ATTRwt-CA group showed significant left ventricular hypertrophy with significantly larger interventricular septum thickness, posterior wall thickness, and left ventricular mass index (A vs G); mitral papillary muscle hypertrophy with significantly larger maximal muscle diameter (B vs H); enlargement of right ventricle with larger basal right ventricular end-diastolic diameter (C vs I) but no significant difference in right ventricular wall thickness (E vs K); and both atrial sizes with significantly larger left atrial volume index and right atrial end-systolic area (D vs J). Notably, compared with those with AL-CA, a significantly smaller proportion presented normal left ventricular wall thickness (interventricular septum thickness and posterior wall thickness ≤ 12 mm) (A vs G). The left ventricular systolic and diastolic function parameters and left atrial strain parameters were not different from those of the AL-CA group. In contrast, their apical-sparing index tended to be higher than the AL-CA group (F vs L). Abbreviations as in **Figure 1**. AL-CA = monoclonal immunoglobulin light chain cardiac amyloidosis; ATTRv-CA = hereditary/variant transthyretin cardiac amyloidosis; ATTRwt-CA = wild-type transthyretin cardiac amyloidosis; BNP = brain natriuretic peptide; IVST = interventricular septum thickness; LA = left atrial; LVEF = left ventricular ejection fraction; LVMI = left ventricular mass index; PWT = posterior wall thickness; RV = right ventricular.

regurgitation but no difference in maximal mitral papillary muscle diameter.

ECHOCARDIOGRAPHIC PARAMETERS DIFFERENTIATING ATTRwt-CA FROM OTHER SUBTYPES OF CA.

Univariate discriminant analysis revealed that advanced age, male sex, non-sinus rhythm, and comorbidities such as hypertension, diabetes mellitus, hyperlipidemia, carpal tunnel syndrome, and paroxysmal atrial fibrillation showed a significant discriminant power differentiating ATTRwt-CA from the other subtypes. Regarding echocardiographic parameters, thickening of IVS and PW, increased left ventricular mass index (LVMI), higher apical sparing index, concomitant more than moderate mitral regurgitation, and enlargement of maximum papillary muscle diameter also showed significant

discriminant power (**Table 3**). Then, the multiple discriminant analysis including these parameters demonstrated that advanced age, male sex, diabetes mellitus, hyperlipidemia, carpal tunnel syndrome, and paroxysmal atrial fibrillation as patient backgrounds, larger LVMI but relatively modest IVS thickening, and papillary muscle hypertrophy as echocardiographic findings had significant discriminant power (**Table 3**). In addition, we provided a figure showing a DP-plot of the discriminant model of ATTRwt-CA, including these parameters with F-value ≥ 2.0 in the multiple discriminant analysis (**Figure 3A**). According to the DP-plot figure, when the sensitivity and specificity are at their maximum values, the discriminant model demonstrated 83.8% discriminant accuracy with 86.0% positive predictive value and 81.4% negative predictive value. (At this

TABLE 3 Parameters Associated With the Diagnosis of ATTRwt-CA

	Multiple Discriminant Analysis		
	F-Value	Discriminant Coefficient (95% CI)	P Value
Age, y	79.4	0.166 (0.129-0.203)	<0.001
Male	11.2	1.487 (0.613-2.360)	<0.001
Non-sinus rhythm	<2.0		
Hypertension	<2.0		
Diabetes mellitus	5.1	1.098 (0.139-2.058)	0.025
Hyperlipidemia	2.8	0.741 (-0.131 to 1.614)	0.095
Carpal tunnel syndrome	19.9	1.954 (1.092-2.817)	<0.001
Paroxysmal AF	3.1	0.775 (-0.089 to 1.639)	0.078
IVST, mm	4.5	-0.185 (-0.357 to -0.013)	0.035
PWT, mm	<2.0		
LVMI,g/m ²	7.8	0.017 (0.005-0.029)	<0.001
Apical sparing index	<2.0		
≥Moderate MR	<2.0		
Maximal papillary muscle diameter, mm	3.2	0.114 (-0.012 to 0.241)	0.075

Abbreviations as in Tables 1 and 2.

point, the theoretical sensitivity, specificity, and accuracy are the same.) In addition, we provided the receiver-operating characteristic curve at the optimal discriminant score where the theoretical sensitivity and specificity match (Figure 3B). When the discrimination score was 0.463, this model showed an AUC of 0.922 (95% CI: 0.890 to 0.954) with a sensitivity of 85.0% and a specificity of 86.6%.

DISCUSSION

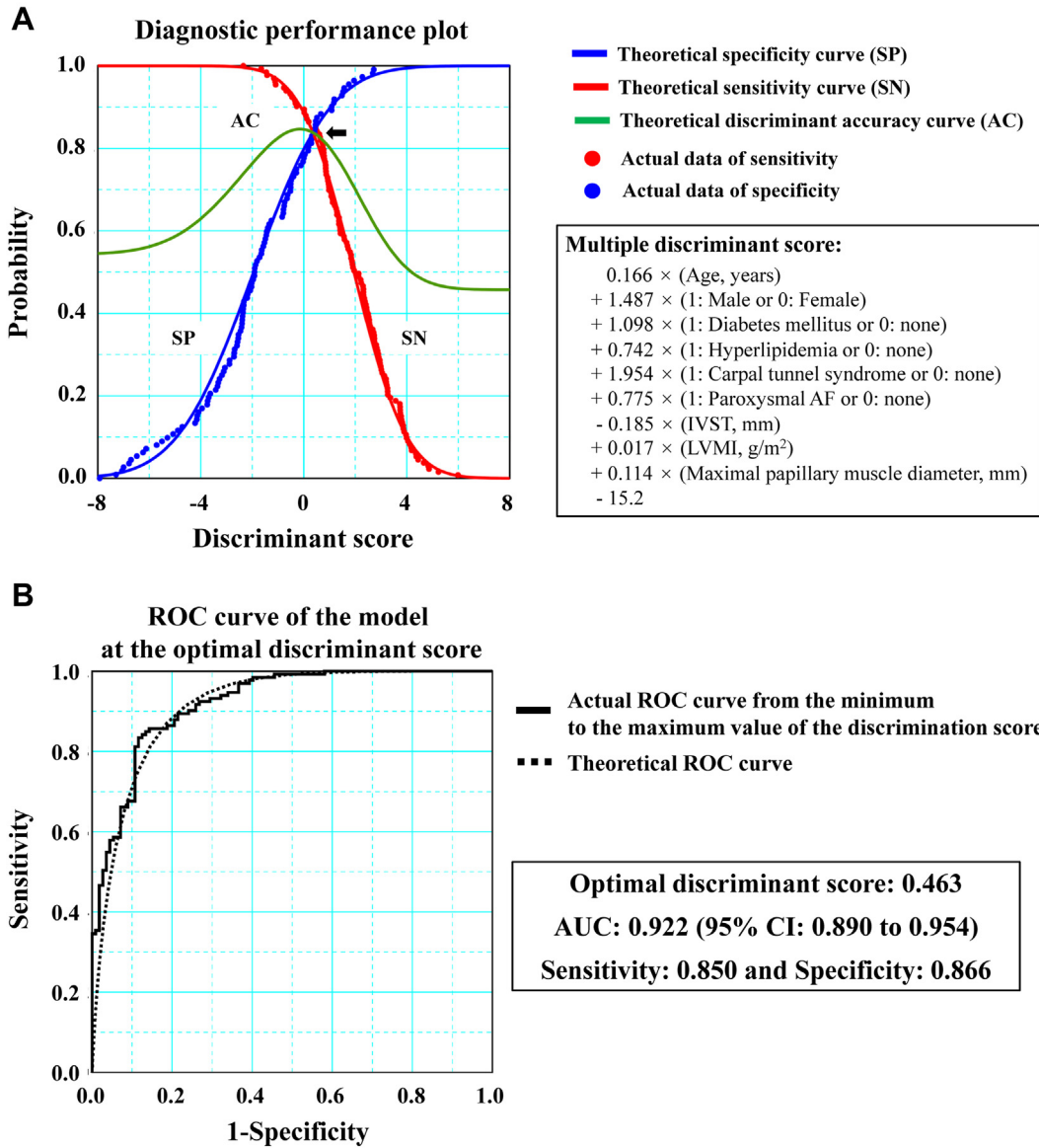
The current multicenter CA survey analyzing the echocardiographic data of patients with histologically proven amyloid deposition within the myocardium demonstrated 3 major findings characterizing ATTRwt-CA. First, compared with patients with AL- or ATTRv-CA, those with ATTRwt-CA were older and more frequently men. They also more frequently presented with non-sinus rhythm and hypertension, diabetes mellitus, hyperlipidemia, carpal tunnel syndrome, or paroxysmal atrial fibrillation as comorbidities. Second, regarding echocardiographic findings, thickening of IVS and PW, increased LVMI, higher apical sparing index, concomitant more than moderate mitral regurgitation, and enlargement of maximum papillary muscle diameter were characterizing ATTRwt-CA. Finally, the multiple discriminant analysis including these patient backgrounds and echocardiographic findings characterizing ATTRwt-CA demonstrated that the patient backgrounds (advanced age, male sex, concomitant diabetes

mellitus, hyperlipidemia, carpal tunnel syndrome, and paroxysmal atrial fibrillation) and the echocardiographic findings (increased LVMI but relatively modest IVS thickening and papillary muscle hypertrophy) showed significant discriminant power differentiating ATTRwt-CA from AL- and ATTRv-CA. (Central Illustration).

In this study, we found 3 impressive echocardiographic findings that characterize ATTRwt-CA. Although LV hypertrophy and relative apical sparing pattern of LS in LV were well-known for identifying CA,^{9,22,23} we found the differences in these findings existed among subtypes of CA and helped differentiate ATTRwt-CA from other subtypes. We also showed that advanced age, male sex, and carpal tunnel syndrome characterize ATTRwt-CA.^{9-11,24,25} With regard to echocardiographic findings, LV hypertrophy is the most common finding for patients with CA.²² The ventricular walls are affected by amyloid deposition and decreased intracardiac volumes, resulting in nondilated concentric hypertrophy. In the current cohort, LV hypertrophy with increased IVST and PWT, increased RWT, and increased LVMI was documented. Patients with ATTRwt-CA presented more intense LV hypertrophy compared with patients with AL- and ATTRv-CA. Increased LVMI was a strongly characteristic finding of ATTRwt-CA in the multiple discriminant analysis. This finding, consistent with previous reports,^{26,27} highlights the dissimilarity in LV wall thickness, with ATTR-CA being thicker than AL-CA. In contrast, one-third of patients with AL-CA were reported to have a normal LV wall thickness (≤ 12 mm),²⁸ which suggests that amyloid deposition is not the only cause of LV hypertrophy. In the current study, 17.9% of patients with AL-CA, but only 6.5% of those with ATTRwt-CA had normal LV wall thickness in regard to both IVST and PWT. Previous reports demonstrated that asymmetrical septal hypertrophy is often noted in ATTR-CA.²⁹ We evaluated asymmetrical septal hypertrophy by calculating the ratio of IVST to PWT and compared the ratio among the 3 subtypes of CA. Patients with ATTRv-CA had a significantly higher ratio than the others, but no difference was found between those with AL-CA and those with ATTRwt-CA.

Amyloid deposits in CA can involve the LV and RV walls, the interatrial septum wall, and heart valves. If the thickness of the RV wall is >5 mm, the amyloid deposits may affect the right ventricle. If the interatrial septum wall has a thickness >5 mm, the amyloid deposits may involve the atria.^{8,30} In the current cohort, cardiac hypertrophic remodeling was also

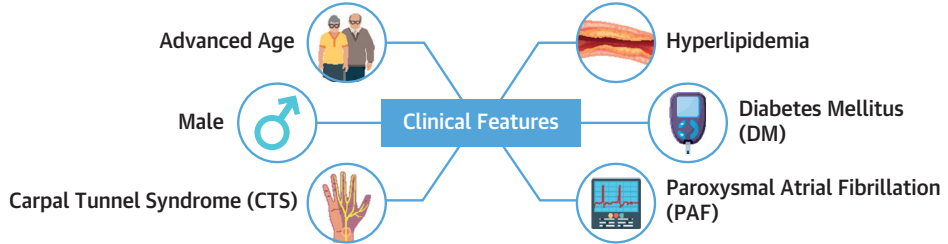
FIGURE 3 Diagnostic Performance of the Discriminant Model of ATTRwt-CA



(A) This figure shows a diagnostic performance plot (DP-plot) of the model with discriminant factors with F-value ≥ 2.0 in the multiple discriminant analysis. The DP-plot diagram demonstrates the sensitivity (red dot) and the specificity (blue dot) when the threshold value is changed from the minimum to the maximum value of the actual data and the theoretical sensitivity (red line), specificity (blue line), and discriminant accuracy (green line) when it is assumed that the data of the 2 groups are normally distributed. When the sensitivity and specificity are at their maximum values (black arrow), the discriminant model demonstrated 83.8% discriminant accuracy with 86.0% positive predictive value and 81.4% negative predictive value. (In this point, the theoretical sensitivity, specificity, and discriminant accuracy are the same.) (B) The receiver-operating characteristic (ROC) curve at the optimal discriminant score where the theoretical sensitivity and specificity match. The actual ROC curve from the minimum to the maximum value of the discrimination score is shown as a solid black line, and the theoretical ROC curve is shown as a dashed black line. When the discrimination score was 0.463, this model showed an area under the curve (AUC) of 0.922 (95% CI: 0.890-0.954) with a sensitivity of 85.0% and a specificity of 86.6%. AF = atrial fibrillation; AC = accuracy curve; SN = theoretical sensitivity curve; SP = theoretical specificity curve.

CENTRAL ILLUSTRATION Echocardiographic Features of Wild-Type Transthyretin Cardiac Amyloidosis

Clinical and Echocardiographic Findings Characterizing ATTRwt-CA



Echocardiographic Features

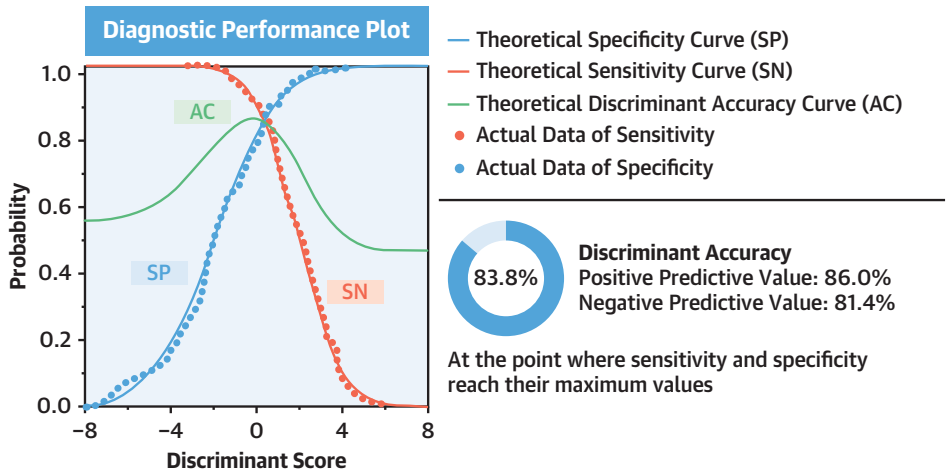


Discriminant Model of ATTRwt-CA From Other Subtypes



Multiple Discriminant Score
 $0.166 \times (\text{age, years}) + 1.487 \times (1: \text{male or } 0: \text{female})$
 $+ 1.098 \times (1: \text{DM or } 0: \text{none}) + 0.742 \times (1: \text{hyperlipidemia or } 0: \text{none})$
 $+ 1.954 \times (1: \text{CTS or } 0: \text{none})$
 $+ 0.775 \times (1: \text{PAF or } 0: \text{none}) - 0.185 \times (\text{IVST, mm})$
 $+ 0.017 \times (\text{LVMI, g/m}^2) + 0.114 \times (\text{maximal papillary muscle diameter, mm}) - 15.2$

Diagnostic Performance of the Discriminant Model



Kitada S, et al. JACC Asia. 2025;5(5):633-646.

J-CASE (Japan Cardiac Amyloidosis Survey of typical Echocardiographic findings) analyzed echocardiographic data in 311 patients with histologically proven amyloid deposition in the myocardium and diagnosis of transthyretin cardiac amyloidosis or monoclonal immunoglobulin light chain cardiac amyloidosis to investigate the echocardiographic findings characterizing wild-type transthyretin cardiac amyloidosis (ATTRwt-CA). The multiple discriminant analysis revealed that, in addition to the patient background, such as advanced age, male sex, diabetes mellitus, hyperlipidemia, carpal tunnel syndrome, and paroxysmal atrial fibrillation, the study found that echocardiographic findings of left ventricular hypertrophy with increased left ventricular mass index (LVMI) but relatively modest interventricular septum thickness (IVS) thickening, and enlargement of maximal papillary muscle diameter demonstrated discriminant power of ATTRwt-CA from monoclonal immunoglobulin light chain cardiac amyloidosis and hereditary/variant transthyretin cardiac amyloidosis. According to the figure showing a diagnostic performance plot of the discriminant model of ATTRwt-CA including these parameters, when the sensitivity and specificity are at their maximum values, the discriminant model demonstrated 83.8% discriminant accuracy with 86.0% positive predictive value and 81.4% negative predictive value.

noted in the RV wall, interatrial septum wall, and heart valves. Among these findings, mitral papillary muscle hypertrophy was more common in patients with ATTRwt-CA than the other 2 groups and, thus, was an important finding characterizing ATTRwt-CA. Although mitral papillary muscle hypertrophy was reported as a valuable finding in distinguishing Fabry disease from other diseases presenting with LV hypertrophy,³¹ there are few reports of this finding characterizing CA. Our research, however, has unveiled its potential in distinguishing subtypes of CA, marking a significant finding that has not yet been reported.

Progressive amyloid deposits prolong LV relaxation in the early stages and increase LV filling pressures with a compensatory LA pressure elevation in the late stages. As the disease advances, more significant amyloid deposits result in a highly rigid ventricular structure, restricting LV filling. In parallel, LV contractility is reduced, and a decrease in the LVEF is eventually noted. Previous reports have shown a decrease in LVEF to $\leq 40\%$ in 30% to 50% of ATTRwt-CA patients at diagnosis.^{5,26} In the current study, the mean LVEF for patients with ATTRwt-CA was $47.4 \pm 11.5\%$, and 25.6% of these patients had an LVEF $\leq 40\%$ at the time of diagnosis. This reduction in the LVEF is a crucial echocardiographic finding suggesting a more severe CA.⁵ Along with LV remodeling, progressive amyloid deposition in the atria results in compensatory remodeling that further increases LV filling pressures with progressive LA dysfunction. This study noted increased E/A and E/e' ratios, enlarged LA volumes, and impaired LA strain parameters, especially in ATTRwt- and AL-CA. However, no echocardiographic finding characterizing ATTRwt-CA was found among LVEF, LV diastolic function parameters, or LA volumes and strain parameters.

The myocardial deformation featuring the amyloid deposit is dual-gradient: basal to apical and sub-endocardium to subepicardial patterns. The sub-endocardial myocardial fibers are responsible for longitudinal deformation. In contrast, subepicardial myocardial fibers are often associated with circumferential deformation.³² LS in the LV, derived from speckle-tracking images, is a unitless measure of longitudinal deformation reflecting the function of longitudinally oriented subendocardial fibers. In our cohort, the global longitudinal strain of the patients was reduced, especially in ATTRwt- and AL-CA.

Although it should be noted that strain parameters decline with age,³³ because most patients with ATTRwt-CA are elderly, that may indicate that LV dysfunction has already progressed at the diagnosis in ATTRwt- and AL-CA. The relative apical sparing pattern evaluated by comparing the basal and mid-segmental LS to the apical LS in the LV has been reported to be a characteristic echocardiographic finding in ATTRwt-CA with high diagnostic accuracy in LV strain parameters.^{9,23} In contrast, recently, similar echocardiographic findings with the relative apical sparing pattern have been documented in non-CA diseases such as end-stage renal disease, hypertrophic cardiomyopathy, and severe aortic stenosis, suggesting that the specificity of the pattern for screening of ATTRwt-CA was obscure.^{34,35} We assessed the relative apical sparing pattern using the equation reported by Phelan et al.²¹ In our cohort, a higher apical-sparing index had a significant discriminant power differentiating ATTRwt-CA from the other subtypes in the univariate discriminant analysis but did not in the multiple discriminant analysis. Regarding its etiology, a basal to apical gradient in myocardial amyloid burden has been reported to have the possibility of association with the pattern.^{32,36} However, Bravo et al³⁷ demonstrated regional differences in the total mass of the amyloid deposition associated with the pattern rather than the proportion of amyloid deposits in AL-CA using 18F-florbetapir positron emission tomography and cardiac magnetic resonance. Additionally, De Gaspari et al³⁸ showed in a histopathologic study on CA that a gradient of amyloid burden from basal to apical did not always explain the pattern. The pattern may be based on complex interactions between amyloid infiltration, amyloid fibril composition, and myocardial structure, which may reduce its specificity in ATTRwt-CA diagnosis.

STUDY LIMITATIONS. First, although this was a multicenter CA survey, the number of patients was relatively small, possibly because CA is a rare disease. In addition, the included patients were limited to those with histologically confirmed amyloidosis deposits in the myocardium and confirmed classification by amyloid immunostaining. Moreover, caused by the nature of being a retrospective study, the limited availability of image data limited the number of echocardiographic findings that could be obtained. As the data analysis included missing values, it is necessary to consider whether the number of data points may have affected the discriminant analysis

results. This study examined the clinical and echocardiographic findings that characterize ATTRwt-CA. Among the patients histologically diagnosed as CA, we discriminated ATTRwt-CA from the other subtypes with high accuracy using echocardiographic findings and several patients' backgrounds. However, we could not gain such a high accuracy in the discrimination based on echocardiographic findings alone. Identifying histological differences among the various subtypes of cardiac amyloidosis can be challenging based on echocardiographic findings alone. Additionally, multiple subtypes of cardiac amyloidosis can coexist within the myocardium,^{39,40} further complicating the ability to discriminate between them using echocardiography. This study found that different subtypes were overlapped simultaneously in the myocardium of 4 of 324 cases (1.2%). When it is challenging to differentiate subtypes of CA by echocardiography, information on patient backgrounds, such as advanced age, male sex, and concomitant carpal tunnel syndrome, may be more helpful.⁴¹ In contrast, LV hypertrophy was one of the primary reasons for suspecting CA in the study patients, and the detection of LV hypertrophy led more than 40% of the patients to a histological examination to diagnose CA. Having the limitations of echocardiographic diagnosis, echocardiographic findings associated with LV hypertrophy and papillary muscle hypertrophy, characterizing ATTRwt-CA, would be essential red flags for the diagnosis of ATTRwt-CA and motivation to the subsequent diagnostic process, including screening a monoclonal component in serum or urine, technetium-99m-pyrophosphate or hydroxymethylene diphosphonate myocardial scintigraphy, cardiac biopsy, and genetic testing. However, future studies are needed to determine the usefulness of these findings in differentiating patients with ATTRwt-CA from those with heart failure with preserved LVEF or aortic stenosis, which have been reported to be frequently associated with ATTRwt-CA.^{42,43} Besides, histological studies are required to clarify further the pathological basis of papillary muscle hypertrophy and the characteristic apical sparing pattern of LS in the LV in CA, which were valuable echocardiographic findings characterizing ATTRwt-CA in our investigation. Unfortunately, this study is a retrospective analysis of patient data that has yet to be fully histologically reviewed on differences in the progression and distribution of

amyloid deposits within the myocardium among subtypes of CA.

CONCLUSIONS

From the J-CASE data set evaluating echocardiographic findings characteristic of ATTRwt-CA, LV hypertrophy with increased LVMI but relatively modest IVS thickening and larger maximal papillary muscle diameter were significant findings. In addition to the patient background, such as advanced age, male sex, and comorbidities (diabetes mellitus, hyperlipidemia, carpal tunnel syndrome, and paroxysmal atrial fibrillation), these echocardiographic findings increased the performance of differentiation of ATTRwt-CA from AL- and ATTRv-CA. The echocardiographic findings characteristic of ATTRwt-CA may lead to more accurate screening echocardiography for diagnosing ATTRwt-CA and motivate the subsequent comprehensive clinical diagnostic process, including multimodality imaging of patients suspected of CA.

ACKNOWLEDGMENTS The authors thank all of the J-CASE investigators who generously provided patient data: T. Sugimoto (Mie University Graduate School of Medicine), Y. Yamada and T. Ishizu (University of Tsukuba), Y. Nabeshima (Saga University), W. Suzuki (Aichi Medical University), M. Tsujiuchi (Showa University Fujigaoka Hospital), T. Nagai (Tokai University School of Medicine), K. Inoue (Ehime University School of Medicine), Y. Takeda (Osaka University Graduate School of Medicine), K. Takahashi (Yawahama City General Hospital), M. Yamano (Kyoto Prefectural University of Medicine), A. Goda (Hyogo College of Medicine), and K. Kusunose (University of the Ryukyus).

FUNDING SUPPORT AND AUTHOR DISCLOSURES

This research was supported by the Academic Project Research Fund of the Japanese Society of Echocardiography. The authors have reported that they have no relationships relevant to the contents of this paper to disclose.

ADDRESS FOR CORRESPONDENCE: Dr Shuichi Kitada, Department of Cardiology, Nagoya City University Graduate School of Medical Sciences, 1, Kawasumi, Mizuho-cho, Mizuho-Ku, Nagoya 467-8601, Japan. E-mail: sikitada0905@gmail.com.

REFERENCES

1. Nienhuis HL, Bijzet J, Hazenberg BP. The prevalence and management of systemic amyloidosis in Western countries. *Kidney Dis (Basel)*. 2016;2(1):10-19.
2. Kitaoka H, Izumi C, Izumiya Y, et al. Japanese Circulation Society Joint Working Group. JCS 2020 guideline on diagnosis and treatment of cardiac amyloidosis. *Circ J*. 2020;84(9):1610-1671.
3. Ton VK, Mukherjee M, Judge DP. Transthyretin cardiac amyloidosis: pathogenesis, treatments, and emerging role in heart failure with preserved ejection fraction. *Clin Med Insights Cardiol*. 2015;8(Suppl 1):39-44.
4. Merlini G, Palladini G. Light chain amyloidosis: the heart of the problem. *Haematologica*. 2013;98(10):1492-1495.
5. Grogan M, Scott CG, Kyle RA, et al. Natural history of wild-type transthyretin cardiac amyloidosis and risk stratification using a novel staging system. *J Am Coll Cardiol*. 2016;68(10):1014-1020.
6. Maurer MS, Schwartz JH, Gundapaneni B, et al. ATTR-ACT Study Investigators. Tafamidis treatment for patients with transthyretin amyloid cardiomyopathy. *N Engl J Med*. 2018;379(11):1007-1016.
7. Cuddy SAM, Chetrit M, Jankowski M, et al. Practical points for echocardiography in cardiac amyloidosis. *J Am Soc Echocardiogr*. 2022;35(9):A31-A40.
8. Ternacle J, Krapf L, Mohty D, et al. Aortic stenosis and cardiac amyloidosis: JACC review topic of the week. *J Am Coll Cardiol*. 2019;74(21):2638-2651.
9. Gillmore JD, Maurer MS, Falk RH, et al. Non-biopsy diagnosis of cardiac transthyretin amyloidosis. *Circulation*. 2016;133(24):2404-2412.
10. Yamamoto H, Yokochi T. Transthyretin cardiac amyloidosis: an update on diagnosis and treatment. *ESC Heart Fail*. 2019;6(6):1128-1139.
11. Inomata T, Tahara N, Nakamura K, et al. Diagnosis of wild-type transthyretin amyloid cardiomyopathy in Japan: red-flag symptom clusters and diagnostic algorithm. *ESC Heart Fail*. 2021;8(4):2647-2659.
12. Miller P, Maurer MS, Einstein AJ, Elias P, Poterucha TJ. Recognizing cardiac amyloidosis phenotype by echocardiography increases downstream testing. *J Am Soc Echocardiogr*. 2023;36(12):1326-1329.
13. Rudski LG, Lai WW, Afilalo J, et al. Guidelines for the echocardiographic assessment of the right heart in adults: a report from the American Society of Echocardiography endorsed by the European Association of Echocardiography, a registered branch of the European Society of Cardiology, and the Canadian Society of Echocardiography. *J Am Soc Echocardiogr*. 2010;23(7):685-713.
14. Lang RM, Badano LP, Mor-Avi V, et al. Recommendations for cardiac chamber quantification by echocardiography in adults: an update from the American Society of Echocardiography and the European Association of Cardiovascular Imaging. *J Am Soc Echocardiogr*. 2015;28(1):1-39.e14.
15. Nagueh SF, Smiseth OA, Appleton CP, et al. Recommendations for the evaluation of left ventricular diastolic function by echocardiography: an update from the American Society of Echocardiography and the European Association of Cardiovascular Imaging. *J Am Soc Echocardiogr*. 2016;29(4):277-314.
16. Adler Y, Charron P, Imazio M, et al. ESC Scientific Document Group. 2015 ESC Guidelines for the diagnosis and management of pericardial diseases: the Task Force for the Diagnosis and Management of Pericardial Diseases of the European Society of Cardiology (ESC). *Eur Heart J*. 2015;36(42):2921-2964.
17. Zoghbi WA, Adams D, Bonow RO, et al. Recommendations for noninvasive evaluation of native valvular regurgitation: a report from the American Society of Echocardiography Developed in Collaboration with the Society for Cardiovascular Magnetic Resonance. *J Am Soc Echocardiogr*. 2017;30(4):303-371.
18. Badano LP, Kolias TJ, Muraru D, et al. Standardization of left atrial, right ventricular, and right atrial deformation imaging using two-dimensional speckle tracking echocardiography: a consensus document of the EACVI/ASE/Industry Task Force to standardize deformation imaging. *Eur Heart J Cardiovasc Imaging*. 2018;19(6):591-600.
19. Cacciapuoli F. The role of echocardiography in the non-invasive diagnosis of cardiac amyloidosis. *J Echocardiogr*. 2015;13(3):84-89.
20. Izumi C, Eishi K, Ashihara K, et al. Japanese Circulation Society Joint Working Group. JCS/JSCS/JATS/JSVS 2020 Guidelines on the Management of Valvular Heart Disease. *Circ J*. 2020;84(11):2037-2119.
21. Phelan D, Collier P, Thavendirathan P, et al. Relative apical sparing of longitudinal strain using two-dimensional speckle-tracking echocardiography is both sensitive and specific for the diagnosis of cardiac amyloidosis. *Heart*. 2012;98(19):1442-1448.
22. Melero Polo J, Roteta Unceta-Barrenechea A, Revilla Martí P, Pérez-Palacios R, Gracia Gutiérrez A, Bueno Juana E, et al. Echocardiographic markers of cardiac amyloidosis in patients with heart failure and left ventricular hypertrophy. *Cardiol J*. 2023;30(2):266-275.
23. Boldrini M, Cappelli F, Chacko L, et al. Multiparametric echocardiography scores for the diagnosis of cardiac amyloidosis. *JACC Cardiovasc Imaging*. 2020;13(4):909-920.
24. Arana-Achaga X, Goena-Vives C, Villanueva-Benito I, et al. Development and validation of a prediction model and score for transthyretin cardiac amyloidosis diagnosis: T-amylo. *JACC Cardiovasc Imaging*. 2023;16(12):1567-1580.
25. Davies DR, Redfield MM, Scott CG, et al. A simple score to identify increased risk of transthyretin amyloid cardiomyopathy in heart failure with preserved ejection fraction. *JAMA Cardiol*. 2022;7(10):1036-1044.
26. Rapezzi C, Merlini G, Quarta CC, et al. Systemic cardiac amyloidoses: disease profiles and clinical courses of the 3 main types. *Circulation*. 2009;120(13):1203-1212.
27. Cipriani A, De Michieli L, Porcari A, Licchelli L, Sinigiani G, Tini G, et al. Low QRS voltages in cardiac amyloidosis: clinical correlates and prognostic value. *JACC CardioOncol*. 2022;4(4):458-470.
28. Lee GY, Kim K, Choi JO, Kim SJ, Kim JS, Choe YH, et al. Cardiac amyloidosis without increased left ventricular wall thickness. *Mayo Clin Proc*. 2014;89(6):781-789.
29. Martinez-Naharro A, Treibel TA, Abdel-Gadir A, Bulluck H, Zumbo G, Knight DS, et al. Magnetic resonance in transthyretin cardiac amyloidosis. *J Am Coll Cardiol*. 2017;70(4):466-477.
30. Dorbala S, Ando Y, Bokhari S, Dispenzieri A, Falk RH, Ferrari VA, Fontana M, et al. ASNC/AHA/ASE/EANM/HFSA/ISA/SCMR/SNMMI Expert Consensus Recommendations for multimodality imaging in cardiac amyloidosis: part 1 of 2-evidence base and standardized methods of imaging. *Circ Cardiovasc Imaging*. 2021;14(7):e000029.
31. Kozor R, Nordin S, Treibel TA, Rosmini S, Castelletti S, Fontana M, et al. Insight into hypertrophied hearts: a cardiovascular magnetic resonance study of papillary muscle mass and T1 mapping. *Eur Heart J Cardiovasc Imaging*. 2017;18(9):1034-1040.
32. Ternacle J, Bodez D, Guellich A, et al. Causes and consequences of longitudinal LV dysfunction assessed by 2D strain echocardiography in cardiac amyloidosis. *JACC Cardiovasc Imaging*. 2016;9(2):126-138.
33. Nakanishi K, Daimon M. Aging and myocardial strain. *J Med Ultrasonics*. 2022;49:53-60.
34. Singh V, Soman P, Malhotra S. Reduced diagnostic accuracy of apical-sparing strain abnormality for cardiac amyloidosis in patients with chronic kidney disease. *J Am Soc Echocardiogr*. 2020;33(7):913-916.
35. Ferreira VV, Rosa SA, Pereira-da-Silva T, et al. Prevalence and prognostic impact of apical sparing contractility pattern in patients with aortic stenosis referred for transcatheter aortic valve implantation. *Am J Cardiovasc Dis*. 2021;11(3):283-294.
36. Sawada N, Daimon M, Abe H, et al. An autopsy case of cardiac amyloidosis with heterogeneous deposition of amyloid protein: a possible

mechanism for relative apical sparing of longitudinal strain. *CASE (Phila)*. 2019;4(2):54-56.

37. Bravo PE, Fujikura K, Kijewski MF, et al. Relative apical sparing of myocardial longitudinal strain is explained by regional differences in total amyloid mass rather than the proportion of amyloid deposits. *JACC Cardiovasc Imaging*. 2019;12(7):1165-1173.

38. De Gaspari M, Sinigiani G, De Michieli L, et al. Relative apical sparing in cardiac amyloidosis is not always explained by an amyloid gradient. *Eur Heart J Cardiovasc Imaging*. 2023;24(9):1258-1268.

39. Kanelidis AJ, Miller P, Prabhu N, et al. ATTR cardiomyopathy meets multiple myeloma: the importance of cardiac biopsy. *JACC CardioOncol*. 2021;3(4):598-601.

40. Gami A, Woller J, Scheel P, et al. Coexistence of light chain and transthyretin cardiac amyloidosis. *JACC Case Rep*. 2024;29(7):102285.

41. Liang S, Liu Z, Li Q, He W, Huang H. Advance of echocardiography in cardiac amyloidosis. *Heart Fail Rev*. 2023;28(6):1345-1356.

42. Castaño A, Narotsky DL, Hamid N, et al. Unveiling transthyretin cardiac amyloidosis and its

predictors among elderly patients with severe aortic stenosis undergoing transcatheter aortic valve replacement. *Eur Heart J*. 2017;38(38):2879-2887.

43. Hahn VS, Yanek LR, Vaishnav J, et al. Endomyocardial biopsy characterization of heart failure with preserved ejection fraction and prevalence of cardiac amyloidosis. *JACC Heart Fail*. 2020;8(9):712-724.

KEY WORDS diagnosis, echocardiography, wild-type transthyretin cardiac amyloidosis